FEATURE ARTICLE

ChemComm
www.rsc.org/chemcomm

Modern microscopy methods for the structural study of porous materials

Michael W. Anderson,*[a] Tetsu Ohsuna,[b] Yasuhiro Sakamoto,[b] Zheng Liu,[bc] A. Carlsson[d] and Osamu Terasaki*[b]

[a] *Centre for Microporous Materials, Department of Chemistry, UMIST, P.O. Box 88, Manchester, UK M60 1QD. E-mail: m.anderson@umist.ac.uk; Fax: +44 161 200 4559; Tel: +44 161 200 4517*

[b] *Stockholm University, 10691 Stockholm, Sweden. E-mail: terasaki@struc.su.se; Fax: +46 8 16 31 18; Tel: +46 8 16 23 79*

[c] *BIO Nanotech Research Institute INC, 3-42-3 Nihonbashi hamacho, Cuo-Ku, Tokyo, Japan*

[d] *Haldor Topsoe A/S, DK-2800 Lyngby, Denmark. E-mail: abc@topsoe.dk*

Received (in Cambridge, UK) 20th October 2003, Accepted 16th February 2004
First published as an Advance Article on the web 4th March 2004

This article describes a number of important recent microscopy tools and their application in particular to the study of porous inorganic materials. The authors believe that these new techniques are on the threshold of delivering enormous new power in the chemist's arsenal for understanding new and complex behaviour in multi-component, hierarchical or composite materials. In particular we consider the contribution of electron crystallography, three-dimensional electron tomography, ultra-high resolution scanning electron microscopy as well as the combined application of high-resolution electron microscopy and atomic force microscopy to the study of surfaces and crystal growth. Much of this work has taken on a particular significance owing to the ground breaking work of scientists at Mobil and in Japan 10 years ago in the successful synthesis of materials with porosity on many length scales achieved through the cooperative self-assembly between inorganic and organic phases. This resulted in a series of materials known as M41S of which MCM-41 and MCM-48 were two of the first and most important structures to be synthesised. This has led to a wealth of new porous structures with order over many length scales and has presented new problems in characterisation. Microscopy methods properly executed are particularly important in the study of this new class of material.

Electron crystallography

Most scientists working with inorganic or organic crystals are accustomed to the ease with which single crystal X-ray structures may be determined. This has in some respects reduced the art of the crystallographer as the process has become more and more automated. Indeed most chemists need not be familiar with the routines which are currently used in order to determine structure directly either from a single crystal or from a powder sample through Reitveld refinement methods. Consequently, in the preamble to this review the reasons why electron crystallography is important and how it may be applied is discussed in some detail. We hope that this will remove some of the mystery surrounding this increasingly important technique. Readers may also wish to refer to a recent related review.[1]

Electron crystallography essentially means solving the crystal structure of a very small single crystal using the diffracted electron beams in an electron microscope. The beam is focused onto a small part of the sample to give a "selected-area electron diffraction" (SAED) pattern. The process is shown schematically in Fig. 1. It is consequently a very useful technique if crystals can only be synthesised on a scale too small for analysis *via* X-rays (*i.e.* typically less than 1 μm). This includes crystals which have a particularly short crystal dimension, as for example needle shaped crystals, and also nano-crystals which are purposely grown at such small scale. Further, as the crystallography is carried out in the electron microscope, in principle, crystallography may be performed on different parts of a sample which varies in composition

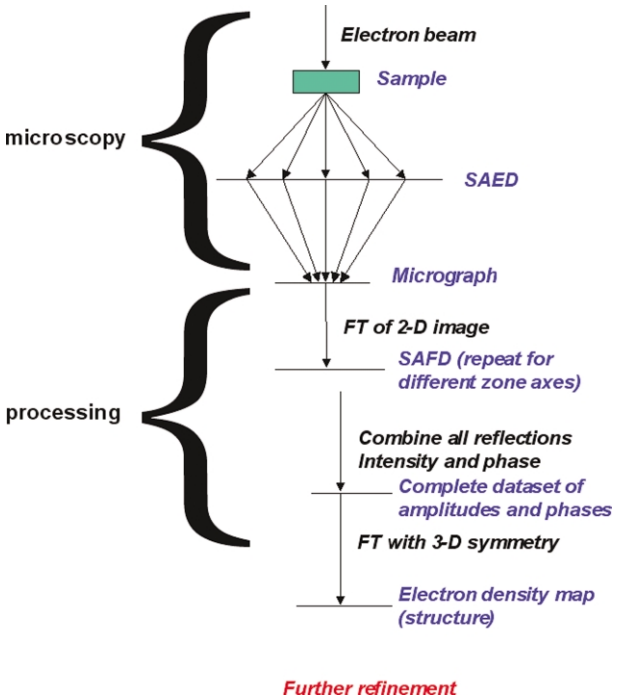

Fig. 1 Schematic of electron crystallography method.

on a sub-micron scale. This is increasingly important in composite materials which, by design, have multiple components within one material. Indeed electron microscopy can also be used to perform a chemical analysis through energy-dispersive X-ray analysis (EDAX) on these sub-micron areas.

There are both advantages and disadvantages to solving a structure by electron crystallography methods as opposed to conventional X-ray diffraction methods. The main advantage has already been discussed concerning the small crystallite size that may be studied. The other main advantage to the electron crystallography method is that because electrons can be focused, unlike X-rays, the diffracted beams, after passing through the crystal may be refocused to form an image (the electron micrograph). This electron micrograph is in essence a hologram constructed from the diffracted beams and carries all the information about the relative phases of the diffracted beams. That is, the micrograph is a result of both the reconstructed amplitude and relative phase of the diffracted beam. Consequently, in electron crystallography it is usual to solve the structure using suitable sections of the electron micrograph rather than the electron diffraction pattern itself. This is known as selected-area Fourier diffractogram diffraction (SAFD). The micrograph in essence becomes the crystal from which the structure is solved. In other words a micrograph is recorded along a suitable zone axis (crystal

DOI: 10.1039/b313208k

direction). Then only a section of this micrograph corresponding to a particularly good part of the sample is chosen (a further selection of area). This section should be as thin as possible to avoid contributions from multiple scattering (which are complex to account for) and where the resolution of the sample is as high as possible. From this section of the micrograph a SAFD pattern may be constructed by straightforward Fourier transformation in two dimensions. But now the diffraction pattern created not only contains the intensity of the diffracted peaks but also their relative phases. In other words all the information from which to calculate the structure of the material. A difficulty, however, arises because there is usually not enough information from one micrograph along one zone axis to solve a structure. For instance a micrograph along the [100] zone axis of a cubic crystal will only contain information about crystal planes parallel to this direction such as for instance [011] or [002]. Consequently in order to collect enough information from which to solve the structure micrographs are usually recorded along several zone axes. In order to balance the relative intensity of the diffraction peaks along different zone axes common reflections must be found between the different directions. This is necessary as inevitably micrographs from different zone axes will be recorded on different crystals with different thicknesses. Having compiled all the reflections, phase and amplitude, this is combined with the 3-dimensional symmetry. A 3-dimensional Fourier transform of this data set leads directly to an electron density map, the structural information. In principle no crystallographic refinement is required as all the information is present to determine the electron density map directly. However, often not all the unique reflections are recorded and therefore the resolution of the electron density map generated is lower than might be expected from a full single crystal X-ray diffraction analysis. Consequently, it is sometimes useful to use the electron density map generated as the starting point for a structural refinement using conventional structural analysis software. This last step depends to some degree on the type of material studied and the information which needs to be collected in order to inform the scientist on a specific problem. For instance, in the structural analysis of ordered mesoporous materials which are only ordered on the nanometer scale and not on the atomic scale a low-resolution electron density map is sufficient to describe the structure and indeed further refinement in such a case would be unproductive.

Zeolites

Recently, Carlsson, Oku *et al.*,[2] have shown for the first time that iron atom positions can be determined inside the framework of a zeolite nano-crystal using electron crystallography (in this case zeolite Y with the faujasite, FAU, framework-type structure). Transition metal nano-particles constrained inside zeolite frameworks have particularly interesting catalytic properties. Fig. 2 shows the refined location of the Fe_6O_n cluster inside the sodalite cage in the FAU structure. In the case of zeolite Y without the iron cluster it was possible to determine the structure using reflections from only two zone axes, [110] and [111]. This resulted in 57 reflections out of a total 101 unique reflections being determine with a resolution which extended out to 1.7 Å. Diffraction patterns were recorded at both 400 kV and 1250 kV the latter being particularly useful as it reduces the chance for multiple scattering and allows somewhat thicker samples to be imaged. Owing to the missing reflections the resolution of the structure map is insufficient to determine the oxygen positions. However, these were found subsequently by using the electron crystallographic density map as a starting position for a refinement of the atomic coordinates using the conventional SHELXTL software. The structure of the iron containing zeolite Y was performed from only one zone axis yielding 38 out of 67 unique reflections extending to a resolution of 2 Å. Although the refinement indicates some discrepancy in the bond lengths as might be expected or determined by X-ray analysis

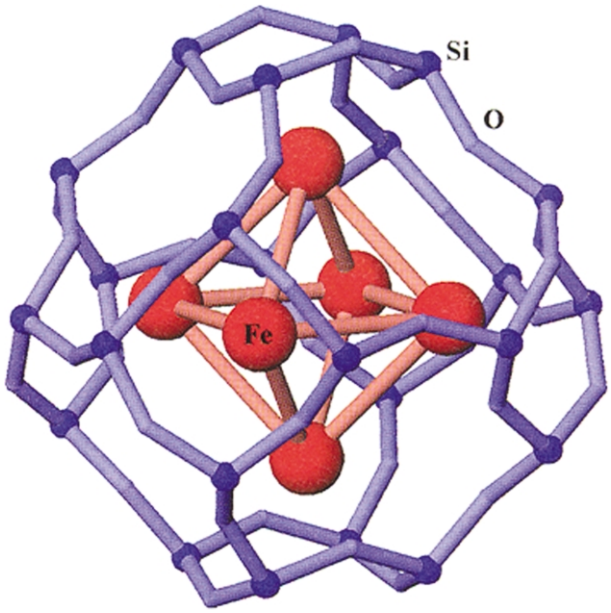

Fig. 2 Refined location of the Fe_6O_n cluster inside the sodalite cage in the FAU structure.[2]

the fit is excellent considering the resolution of the data set and certainly sufficient to locate the position and connectivity of the iron cluster. Such structures can of course also be used as starting positions for further analysis and refinement by computational methods.

SSZ-48 is a novel large-pore high silica zeolite synthesised by workers at Chevron Research and Technology group. The structure solution by electron crystallography recently, Wagner *et al.*,[3] represented the most complex three-dimensional material to be solved to atomic resolution by electron crystallography to date. Fig. 3 shows the nano-sized needle-like crystal fibres of SSZ-48 with size *ca.* 0.05 μm × 0.25 μm × 10 μm. Such crystals are below the dimensions accessible for standard single-crystal X-ray analysis. In order to determine this complicated structure integrated intensities for 600 reflections (326 of which are unique) were extracted from 11 zone axes of selected area electron diffraction data to a resolution of 0.99 Å. These were merged in the normal way described above and the cell indexed to a monoclinic crystal class

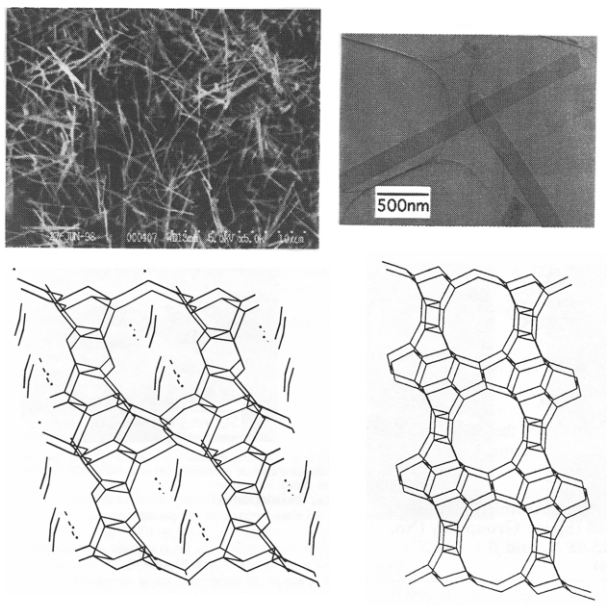

Fig. 3 Nano-sized needle-like crystal fibres of SSZ-48 with structural refinement.[3]

consistent with space group $P2_1$ (group 4 with very little symmetry). The full structural refinement was performed in two stages. First an electron density map was generated using the amplitudes and phases of 157 of the reflections generated in the SAFDs — these were considered to be the most reliable reflections with sufficient intensity. The 3-dimensional potential map easily revealed the 7 unique silicon atoms in the unit cell as well as 5 of the 14 oxygen atoms. Additional electron density within the pores could be attributed to the organic templating agent (*N*,*N*-diethyl-decahydroquinolinium) used in synthesis and 9 carbon positions ascribed. The remaining oxygen atoms were then positioned using a distance-least-squares refinement (DLS) to optimize Si–O bond distances and O–Si–O bond angles. This yielded all 14 oxygen positions. The second step of the refinement was to use these atomic coordinates as the starting point for a Reitveld refinement of experimental synchrotron X-ray powder data. This complete structural refinement resulted in both accurate framework positions but also location of the organic templating agent providing a valuable insight into the inorganic–organic interactions in this 12-membered ring zeolite.

A modification of the general procedure is described when data is of insufficient quality to unambiguously determine structure. Liu *et al.*[4] and Ohsuna *et al.*[5] describe the structural solution of polytype C of nano-crystalline zeolite beta known as ITQ-14 and assigned the structure code BEC. Zeolite beta is a very important zeolite in that it is one of only a handful of structures that possesses large 12-membered rings in three dimensions. This gives zeolite beta particularly good diffusion properties for catalysis. However, zeolite beta normally crystallises as an intergrowth structure of a number of theoretical polymorphs. One polymorph is particularly interesting because it has a spiral 12-membered channel running in one direction. Synthesis of this polymorph has eluded scientists which might be particularly interesting for chiral separation of catalysis. However, recently another non-chiral polymorph was synthesised, polymorph C, which may give clues to the synthesis of the chiral variant. The papers by Liu *et al.*[4] and Ohsuna *et al.*[5] describe the procedure to elucidate and confirm that the new crystals were indeed the polymorph C of zeolite beta.

The crystals to be analysed occurred as small pillars only 50 nm in section attached to much larger crystals which turned out to be normal intergrown zeolite beta. Hence it was appropriate to use electron crystallographic methods in order to solve the crystal structure. See Fig. 4 which shows diffraction patterns and electron micrographs from the bulk zeolite beta and the nano-crystals of ITQ-14. SAFDs were generated from micrographs along 7 zone axes yielding 1618 total reflections including symmetrically equivalent ones. After compiling a suitable data set in the normal manner the 3-dimensional electron density map was generated. However the framework generated was incomplete and required completing using DLS methods. However, this yielded a number of possible solutions to the framework connectivity. In order to improve the quality of the electron density map a new procedure was employed.

Fourier transform directly of the SAED pattern in the absence of phase information yields a Patterson map. This is a map which gives information not about atomic positions (as the phases are absent) but about vector separations between atoms. This information can be used to enhance the quality of the 3-dimensional electron density map in a very clever manner. A duplicate electron density map is added to the electron density map but shifted by an atom–atom vector. Consequently, one atom moves on top of a neighbour and the electron density in this position is enhanced. Another duplicate is added shifted in the opposite sense thereby enhancing the electron density the first atom. By continuing this process for all known interatomic vectors the electron density at atom positions is enhanced thereby helping to locate atom centres. This method is given the name Shift-Overlap Multiply Enhancement Method (SOMEM). The authors first test the method on the well understood structure of zeolite A. Then by applying the method to the data set in this example the framework connectivity and atomic coordinates of polymorph C of zeolite beta were unambiguously determined.

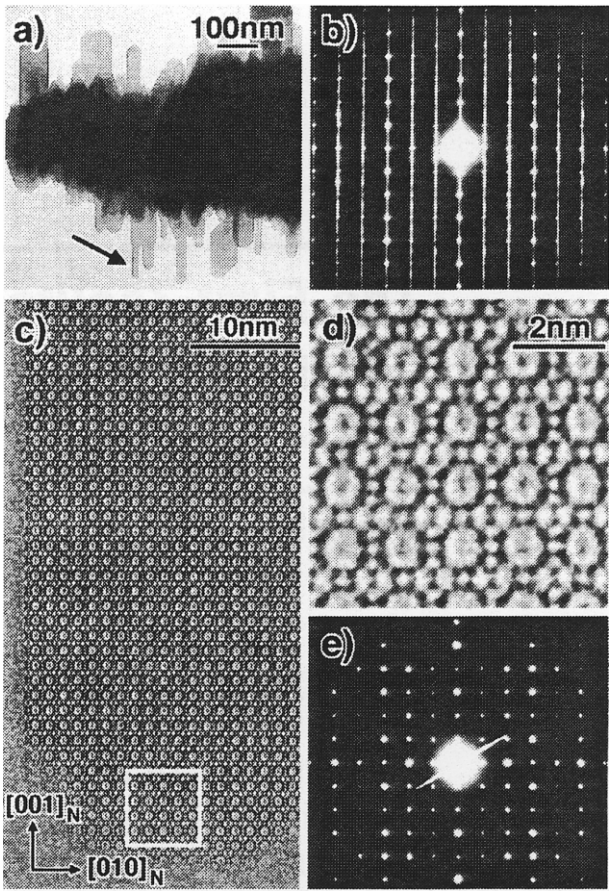

Fig. 4 Diffraction patterns and electron micrographs from the bulk zeolite beta and the nano-crystals of ITQ-14.[4,5]

Mesoporous materials

Ten years ago a very important new class of mesoporous material was developed simultaneously by scientists in Mobil Corporation and in Japan. An archetypal material in this class is MCM-41 which is a mesoporous hydrated silicate with unidimensional pores in a hexagonal arrangement. The ordering in these types of material is created by the cooperative assembly with an organic surfactant which forms a liquid crystalline mesophase template around which the inorganic material solidifies. The walls of the inorganic phase are generally amorphous in nature and the ordering is only present on the meso-scale, between 1.5 nm and 30 nm. By changing the length of the surfactant molecule pore sizes can be tuned. By changing the surfactant or by using a block-copolymer or by changing the synthesis conditions a whole variety of pore architectures may be formed. These types of material can be highly ordered on the meso-scale with two or three-dimensional symmetry and even crystal-like morphology. Fig. 5 shows two electron micrographs of SBA-1 and SBA-6, symmetry $Pm\bar{3}n$, which both have nominally the same pore and cage structure (see Sakamoto *et al.*[6] and Che *et al.*[7]). The micrographs are reproduced with the same relative scale to illustrate how different pore sizes can be achieved within the same structure type. SBA-6 with the larger pores is synthesised using $C_{18}H_{37}OC_6H_4OC_4H_8N(CH_3)_2C_3H_6N(CH_3)_3Br_2$ as templating agent and SBA-1 with the smaller pores uses cetyltriethylammonium bromide as templating agent. The unit cell for SBA-6 is 160 Å compared with 86 Å for SBA-1.

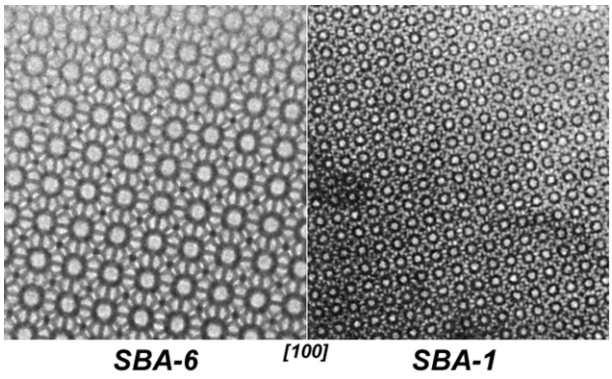

Fig. 5 Electron micrographs of SBA-1 and SBA-6 along [100].[6,7]

However, the X-ray diffraction of such materials does not contain much information and can not easily be refined without a structural model. Electron microscopy takes on a special significance for such materials which can be illustrated by the vast number of images of different materials which have appeared in the literature over the last decade. Further, electron crystallography has become key to solving, *ab initio*, the wall topology of a variety of these new structures. A similar procedure is used to that described previously for atomically ordered crystals. However, the number of reflections and consequently the resolution will be much lower as the ordering is on a much longer length scale.

Nevertheless, Sakamoto *et al.*[6] were able to determine 42 out of 44 unique reflections for SBA-6 to a resolution d = 21 Å. In order to collect such data the microscope is operated at very large underfocus conditions of several thousand Angstroms which is very different to the conditions traditionally used for atomic resolution of crystals. Three-dimensional Fourier transform leads to an electron density map where the density defines the difference between the wall structure and the pore. The position of the boundary between wall and pore could be judged from the electron density map but this would probably have significant error. To overcome this problem additional information is used from gas adsorption measurements. The total pore volume is known from nitrogen adsorption to be V_p = 0.86 cm^3 g^{-1} and the wall density is known from helium picnometry to be D_w = 2.2 g cm^{-3}. Together this yields quite accurately the ratio of the volume of the pore to that of the wall. Using this information the threshold in the electron density map between wall and pore can be determined to give the same volume ratios. Fig. 6 shows the final result of this wall structure determination for SBA-6.

SBA-6 exhibits a bimodal three-dimensionally interconnected cage system with cage sizes 73 Å and 85 Å respectively. SBA-1 has essentially the same structure but with about half the unit cell size of SBA-6. These structure solutions *via ab initio* methods are the first reported for this new class of mesoporous material. The bimodal cage system in SBA-1 and SBA-6 can be viewed in a number of ways. A clathrate structure can be built of two space filling cages, a tetrakaidecahedron (14-hedron with 10 pentagons and two hexagons) and a pentagonal dodecahedron (12-hedron all pentagons), see Fig. 6. The ratio of the two cage systems is three : one respectively. Interestingly recently Weaire and Phelan[8] showed that by distorting these regular hedra slightly to give curved edges and curved faces space could be partitioned into two equal volumes in a more energy efficient way that proposed by Lord Kelvin in 1887 using distorted truncated octahedra. Also recently Anderson *et al.*[9] have shown that the structure of SBA-1 can be built from spherical and ellipsoidal bodies representing the templating micellar surfactant and described by an analytical function in a similar manner to MCM-48, also see Fig. 6. This further demonstrates that solving the structures of mesoporous materials holds lessons for the structures of surfactants. Owing to the dynamic nature of surfactant mesophases their structures are hard to

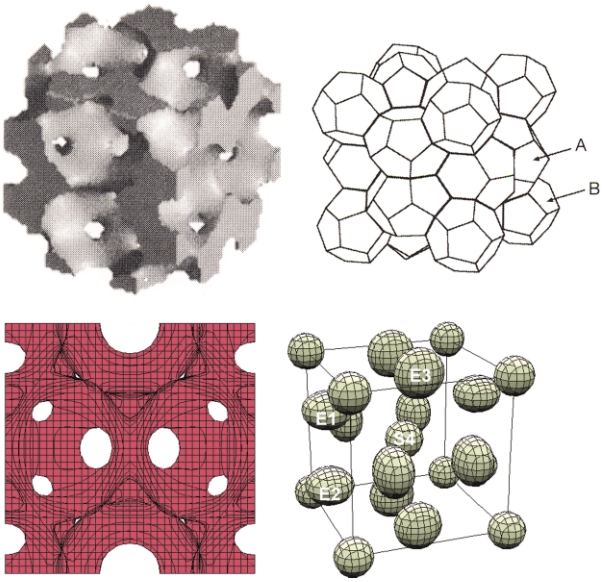

Fig. 6 Structure of SBA-1 or SBA-6 observed as an electron density and described either in terms of a clathrate structure or as a surface enveloping the micellar templating agents.[6,9]

solve and this has resulted in lengthy discussions in the literature. Mesoporous silica materials represent a frozen version of the surfactant phase which can then be studied at leisure. SBA-1 is an excellent example how the subtle details of the surfactant I1 structure are captured in the silicate replica.

The same paper also discusses the structure solution of SBA-16, symmetry $Im\bar{3}m$, which is shown to be a body-centered arrangement of cages with diameter 95 Å connected through large windows with diameter 23 Å along the [111] directions. The surface of SBA-16 is related to the minimal surface I-WP and can be described by the simple analytical function $(\cos\pi x \times \cos\pi y) + (\cos\pi x \times \cos\pi z) + (\cos\pi y \times \cos\pi z) = 0$.

SBA-12 is a mesoporous silicate material synthesised using a non-ionic oligomeric ethylene oxide surfactant Brij76($C_{18}EO_{10}$). The resulting material exhibits a very poorly defined X-ray diffraction pattern and yet displays excellent ordering in the electron microscope. The appearance of the micrographs, see Sakamoto *et al.*,[10] indicates an intergrowth structure which is typical for cubic/hexagonal close-packed systems. The SAED pattern always contains diffuse streaking consistent with such an intergrowth. By carefully selecting a region of a micrograph without intergrowth it was possible to obtain a SAFD containing information about a pure polymorph with no streaking. This aids the structural refinement considerably and illustrates the additional power of electron crystallography for determining the structure of intergrowth systems. Ten reflections could be indexed from this section and after treatment in the usual manner an electron density map indeed revealed a cubic close-packed cage structure for SBA-12. The material is interspersed with twin planes creating short sections of a hexagonal polymorph.

One of the first mesoporous materials to be synthesised by Mobil Corporoation was MCM-48. The structure of MCM-48 is based on a bicontinuous cubic surfactant phase with symmetry $Ia\bar{3}D$ shown in Fig. 7. In other words the wall structure is a continuous surface which wraps three-dimensionally in a cubic arrangement. The wall encloses and separates two chiral channel systems with opposite handedness. Although the structure had been inferred from modelling studies and fitting of powder X-ray profiles and HREM images, Alfredsson and Anderson,[11] previously it is only recently that the structure has been confirmed by direct *ab initio* electron crystallographic methods, Kaneda *et al.*[12] The method of Alfredsson and Anderson was to describe the surface of MCM-48 by an analytical function closely approximating the gyroid minimal

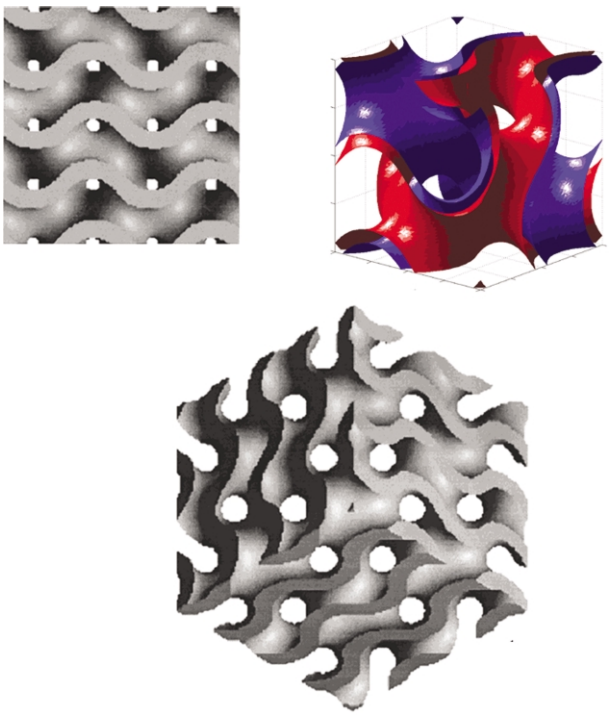

Fig. 7 Electronic density maps and bicontinuous cubic structure of MCM-48.[11,12]

surface ($\sin\pi x \times \cos\pi y$) + ($\sin\pi z \times \cos\pi x$) + ($\sin\pi y \times \cos\pi z$) = 0. This would result in an infinitesimally thin wall. Wall thickness is generated by allowing the function to vary between $\pm\delta$ and this becomes a parameter refinable against powder X-ray diffraction, for instance.

Mesoporous silica materials are in themselves useful templates to further inorganic structures. In particular it is possible to synthesise inorganic carbon replicas *via* catalytic carbonisation of carbon sources such as sucrose, fufuryl alcohol or acetylene. Following synthesis of the carbon replica the silica substrate can be removed by dissolution in sodium hydroxide or hydrogen fluoride. The resulting structure is a very stable high surface area carbon support with ordered mesoporosity. This technology has been developed by Ryoo in Korea (Ryoo *et al.*[13]). For instance, using MCM-48, symmetry $Ia\bar{3}d$ as substrate two carbon networks may be synthesised, CMK-1 from sucrose (Carbon Material KAIST-1) with symmetry $I4_132$ and CMK-4 from acetylene with symmetry $Ia\bar{3}d$. The HREM images of CMK-4 are shown in Fig. 8 along the three zone axes [100], [110] and [111] (Kaneda *et al.*[12]). A total of eight structure factors could be determined for CMK-4 and it is interesting to note that the phase relation is exactly the opposite as for MCM-48 (using the same origin for the calculation. This is expected for a material which is a negative reversal of the original structure. The structure for CMK-4 is also illustrated in Fig. 8 and is shown to be a three-dimensionally interconnecting rod system which mimics the original surfactant structure used to synthesise the silica framework. The rod diameter is estimated to be in the region of 30 Å and this is determined without the use of gas adsorption measurements in this case.

CMK-1 which is synthesised using sucrose as template shows a substantially different topology in the electron micrographs. A domain structure exists and in no region is the structure similar to CMK-4. It is shown by Kaneda *et al.*[12] that in CMK-1 the two rod networks are not stabilised relative to one another and this results in a shift of the networks along [100] until they touch. The domain-like appearance is caused by different domains shifting along equivalent < 100 > directions.

Apart from carbon many other important materials may be grown inside mesoporous templates. For example mesoporous Pt nano-

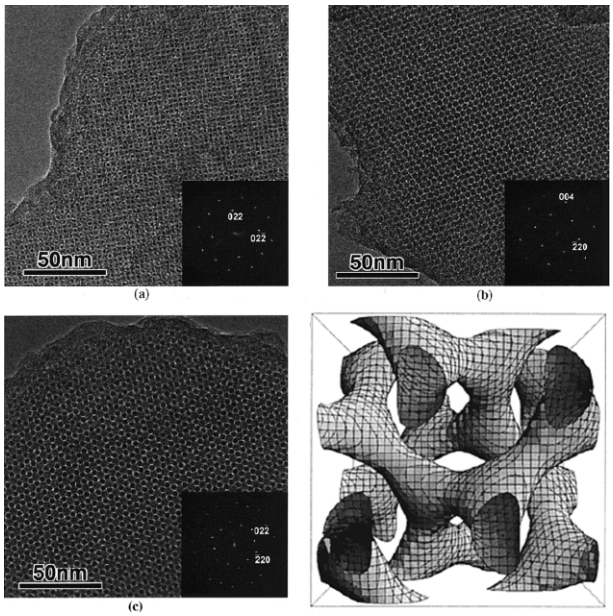

Fig. 8 HREM images of CMK-4 along the three zone axes [100], [110] and [111] together with a representation of the carbonaceous surface.[12]

wires may be grown inside MCM-41, SBA-15 and MCM-48. These have all been reviewed by Terasaki *et al.*[14] and this reveals that the nanowires may be successfully extracted from the mesoporous silica template. Fig. 9 shows an example of Pt nanowires grown inside MCM-48 and the mesoscopic structure of the nanowires is essentially the same as that of CMK-4 shown in Fig. 8. Interesting the Pt nanowires are formed predominantly inside only one of the non-intersecting channel systems and consequently are chiral. The arrows in Fig. 8 indicate regions where both channels are filled and the Pt nanowire assumes two intertwined opposite handed rod structures.

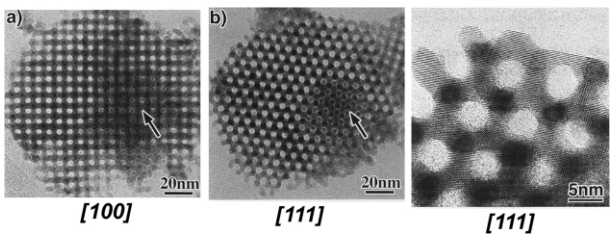

Fig. 9 Pt nanowires grown inside MCM-48.[14]

The future in structure solution by electron microscopy techniques may lie in a different approach to structure solution Miao *et al.*[15] This paper concerns a theoretical description of a new way to operate the electron microscope which should be possible in the very near future. The trick comes in being able to use the electron diffraction pattern to calculate structures (similar to the direct methods used in X-ray diffraction measurements). But in order to do this a method is required to extract the phase relationships in the diffracted beams in a simple manner without going through the electron micrograph. The method proposed involves having a highly parallel electron beam which is capable to collect a diffraction pattern from an area larger than the total crystallite. Consequently the diffraction pattern, if sampled at a high enough resolution (the over-sampling method) will consist of not only diffraction from the crystal by diffraction from outside the crystal — which should be zero. Consequently a two dimensional Fourier transform of the diffraction pattern with the correct phase set would reveal not only the periodicity within the crystal but also a set of zeroes around the crystal. If the wrong phase relations are used then electron density will be observed in the non-allowed regions outside the crystal. Consequently, a method is introduced to

iteratively determine the correct phase relationships. When these are correctly determined a full collection of diffraction patterns at many incidence angles will provide enough information to solve structure to atomic resolution by direct methods. Miao *et al.*[15] demonstrate theoretically how this should be possible for zeolite A. This technique is under development and hopefully the first results will be encouraging.

3D-TEM, electron tomography

Electron crystallography, as described in the previous section, relies on a "crystallographic" periodicity within the object. Many materials, however, have composition which varies on a nanoscopic scale in a manner which is non-periodic. For instance metal particles dispersed on a catalytic support or mesoscopic voids which provide diffusion pathways in "real working" catalysts. A technique which is ideally suited to the task of monitoring such phenomena is three-dimensional electron tomography (or 3D-TEM). 3D-TEM has been used for some time to study biological systems but the application to materials science is just beginning to be realised. Two groups in particular have been instrumental in redirecting this technique to the study of materials, that of Midgley, Weyland and Thomas in Cambridge and de Jong *et al.* in Utrecht. The process of TEM relies on the ability to record an extensive tilt series of micrographs over a wide angular range. Typically 140 micrographs are recorded over an angular range ±70° using an automated data collection system which permits recording of digital images with automatic compensation of image shifts and focus variations that occur during tilting. Such a large 2-dimensional data stack recorded over a wide angular range contains complete information about the 3-dimensional mesoscopic non-periodic topology of the system. In order to reconstruct the 2-dimensional data stack into a three dimensional image requires first proper alignment of the images followed by Fourier transform, reconstruction and inverse Fourier transform. Proper alignment is most easily achieved in the presence of a high scattering marker such as a 5 nm gold bead. The resolution d of the 3D image can be approximated by $d = \pi(T/N)$, where N is the number of projections and T the thickness of the sample.

Koster *et al.*[16] applied the 3D-TEM approach to the study of silver particles on a zeolite Y and mesoporous generated in zeolite mordenite through acid treatment. Metal loaded zeolites have catalytic applications in catalytic reactions such as hydro-isomerisation. However, the distribution of the metal particles within the microporous crystallites is crucial to their catalytic performance. 3D-TEM is ideally suited to the task and the authors demonstrate that they can locate 10–40 nm silver particles both at the external surface of the zeolite crystals and also buried within the crystals. Observation of metal particles has the added advantage that markers for alignment are already present and do not have to be added to the system. In this paper seven silver particles were used as markers for alignment purposes.

Real working zeolite catalysts are often pre-treated by steaming or acid leaching in order to generate mesoporosity within the crystals. This essentially destructive process is crucial to provide rapid access to the internal spaces of the zeolite. However, as the process is not very specific the result is a highly disordered type of mesoporosity which is extremely difficult to quantify. 3D-TEM is shown to be probably the first technique to reveal the details of such a process and is consequently going to be extremely important in catalyst development in the near future. Koster *et al.*[16] demonstrate mesoporosity in acid leached mordenite which is particularly useful as a catalyst for aromatics alkylation. Of course the two dimensional representation of the results in publication do not do justice to the power of 3D-TEM as it is important to view 3-dimensional moving images to capture the full impact of the technique. However, fortunately such images are always available on the internet in supporting documents to the publications (see in this instance http://pubs.acs.org). Two excellent subsequent papers Janssen *et al.*[17] and Janssen *et al.*[18] further demonstrate the application of 3D-TEM to the study of mesopore formation in hydrothermally treated zeolites. Fig. 10 shows theoretical diffusion lengths in microporous crystals through the micropores in the presence and absence of different types of mesoporosity and a 3D-TEM slice showing cylindrical pores in hydrothermally treated zeolite Y is also shown (again see http://pubs.acs.org for moving images). Fig. 11 shows a montage of trapped mesopores in a zeolite Y crystallite.

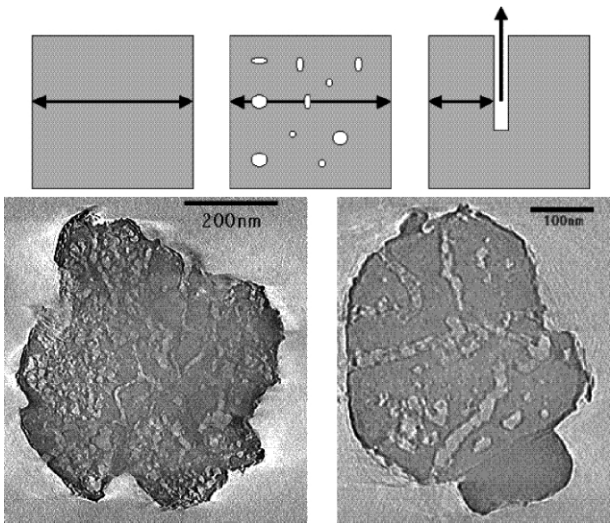

Fig. 10 Theoretical diffusion lengths in microporous crystals through the microporous in the presence and absence of different types of mesoporosity and a 3D-TEM slice showing cylindrical pores in hydrothermally treated zeolite Y.[18]

Another important development in 3D-TEM is Z-contrast tomography which has been illustrated by Midgley *et al.*,[19] Weyland *et al.*[20] and Midgley *et al.*[21] This technique makes use of the high contrast that can be achieved from Rutherford scattered electrons from high atomic mass elements. Rutherford scattering at high angle is proportional to Z^2 and consequently with a detector which collects specifically at high angle (known as high-angle annular dark field HAADF) detector the scattering from for instance metal nanoparticles in catalytic particles may be enhanced. The Z-contrast tomography has been applied to Pd_Ru on mesoporous silica supports and Pd on carbon supports where the support is low atomic mass and the catalytic nanoparticle has high atomic mass. An example of Pd_Ru particles dispersed on a mesoporous silica support are shown in Fig. 12 with the metal particles highlighted in red to improve the visual impact.

Finally Janssen, Voort *et al.*[22] have demonstrated that the 3D-TEM technique can also be used to determine the tortuosity of mesopores in ordered mesoporous materials of the MCM type. They have applied the technique to SBA-15 which is a wide pore version of the hexagonal unidimensional pore system in MCM-41. The pore diameter in SBA-15 is *ca.* 8 nm and 3D-TEM clearly demonstrates that in larger particles the hexagonally arranged pores fold back on themselves in to U-shaped channel systems. It is likely that 3D-TEM will be particularly useful in the future for the study of this important class of material.

Ultra-high resolution SEM

In principle scanning electron microscopy has advantages over transmission electron microscopy for the study of surface structure and also in terms of ease of use. However, SEM is limited in resolution owing to charging effects on the sample. However, the technology for working at very low currents and voltages now allows SEM and STEM images to be recorded with nanometer

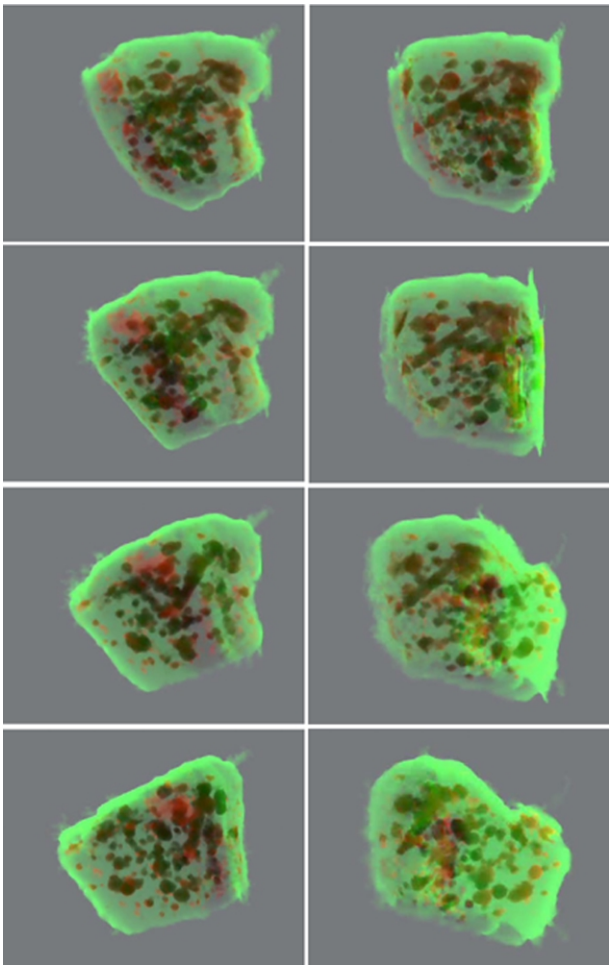

Fig. 11 Montage of trapped mesopores in a zeolite Y crystallite.[18]

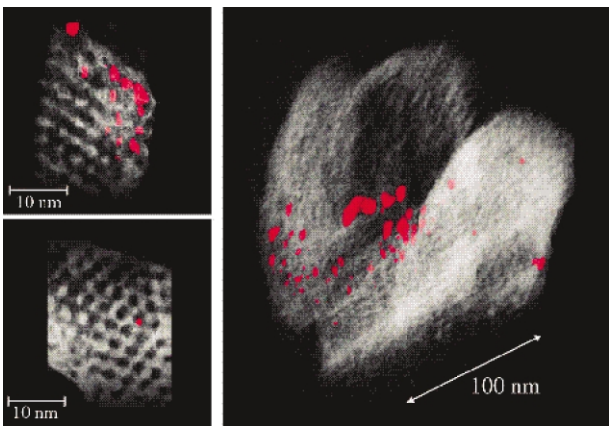

Fig. 12 Pd_Ru particles dispersed on a mesoporous silica.[21]

resolution on inorganic oxide materials. A stunning illustration of the potential of the technique is shown in Fig. 13 which shows surface structure in the mesoporous silicate SBA-15 with pore size 8 nm — Che *et al.*[23] The pores can clearly be imaged and the wrapping of tunnel structures is evident.

Surface structures by HREM and AFM

Microscopy methods are also suited to the study of surface structure in porous materials. This is particularly important in the investigation of crystal growth in framework inorganic materials such as zeolites. In this respect a combination of high-resolution electron microscopy of surface structure, atomic force microscopy and

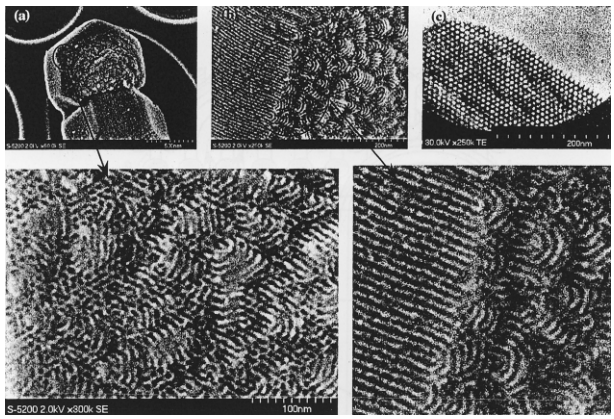

Fig. 13 Ultra-high resolution SEM of the surface structure in the mesoporous silicate SBA-15 with pore size 8 nm.[23]

theoretical modelling is beginning to reveal import features about crystal growth. At present HREM is the only experimental technique which can determine the details of the surface structure by observing at high resolution across the surface of the crystal. In particular for zeolites work has been conducted on zeolite Y (Alfredsson *et al.*[24]) zeolite L (Ohsuna *et al.*[25]) and polymorph C of zeolite beta (Slater *et al.*[26]). In the case of zeolite Y seen in Fig. 14 it has been shown that the preferred surface termination is through a double or single six-ring structure. In zeolite L which has hexagonal symmetry the crystals are hexagonal rods. Careful HREM at the surface revealed (as shown schematically in Fig. 15 the (001) face is terminated with a double six-ring and the side walls (100) is terminated with a closed cancrinite cage structure. The appearance of closed cage structures at the surface of zeolites seems to be a feature common to many of the HREM studies. The surface structure of polymorph C of zeolite beta has been studied recently by a combination of high-resolution electron microscopy and

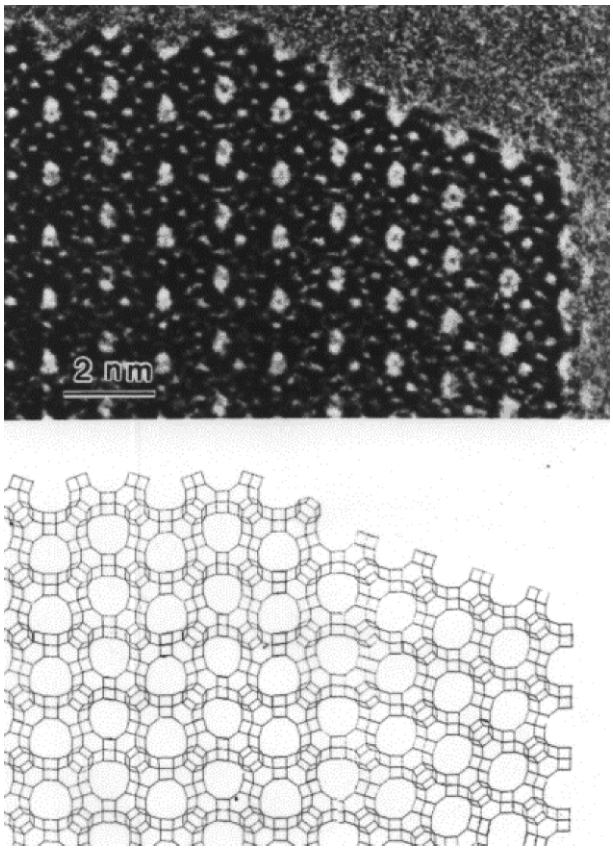

Fig. 14 Preferred surface structures observed in an intergrowth system of zeolite Y indicating the importance of double 6-ring terminations.[24]

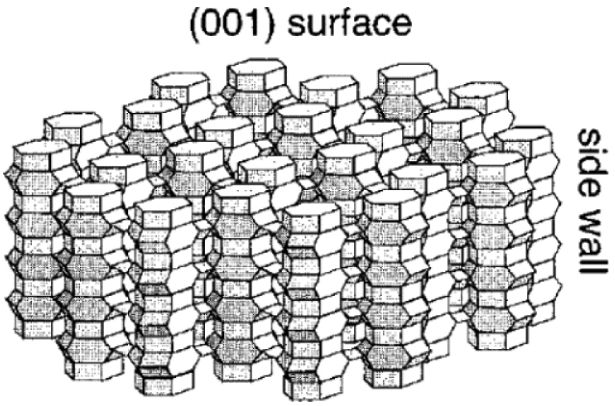

Fig. 15 Surface structure of zeolite L determined from electron microscopy. The (001) face is terminated with a double six-ring and the side walls (100) is terminated with a closed cancrinite cage structure.[25]

modelling of surface energies, see Slater *et al.*[26] Fig. 16 shows the two surface structures observed by HREM together with the computed electron micrographs. The energetic calculations are generally in agreement with experiment and implicate a double four-ring unit in the growth mechanism for this structure. We predict that comparisons such as these between HREM data on surface structure and theoretical calculations of attachment energies or equilibrium morphologies will be important for understanding crystal growth phenomena. It is important, however, at this stage to use as much experimental evidence as possible in order to substantiate the theoretical measurements in order to increase the confidence for a predictive use of theory in such studies in the future.

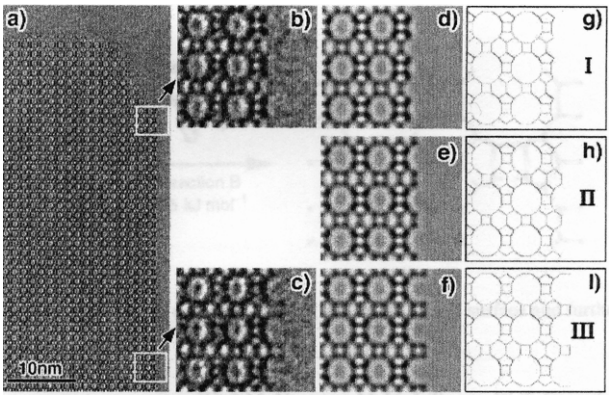

Fig. 16 The surface structure of polymorph C of zeolite beta studied by a combination of high-resolution electron microscopy and modelling of surface energies.[26]

Another very powerful microscopy tool for observing surface structure in porous crystalline material is atomic force microscopy (AFM). This technique is ideally suited to the task of characterising very shallow terraces on the surface if crystals as the vertical resolution is on the order of 1 Å and the lateral resolution (which does not need to be as high) is *ca.* 20 Å — although periodic structures can be resolved to molecular or even atomic resolution. AFM also has the further advantage that it can be performed under air or under solution and therefore, in theory, it should be possible to measure surface structure changes in situ during crystal growth. This has yet to be achieved for open-framework systems — mainly due to the growth conditions — but has already been demonstrated for a number of molecular crystals.

Crystal growth can occur by a number of mechanisms. Two very common growth mechanisms in dense phase crystals is layer growth and spiral growth. In layer growth a surface terrace is nucleated on the surface of a crystal and then propagates by addition of nutrient at the edge of this terrace. In spiral growth nutrient is added along the edge of a spiral terrace emanating from a screw dislocation. In open framework materials the main type of growth phenomenon is layer type growth although there are a couple of reports of spiral growth. One such report is for the natural mineral heulandite (Yamamoto *et al.*[27]) and the AFM of the [010] surface is shown in Fig. 17. A very clear growth spiral is observed

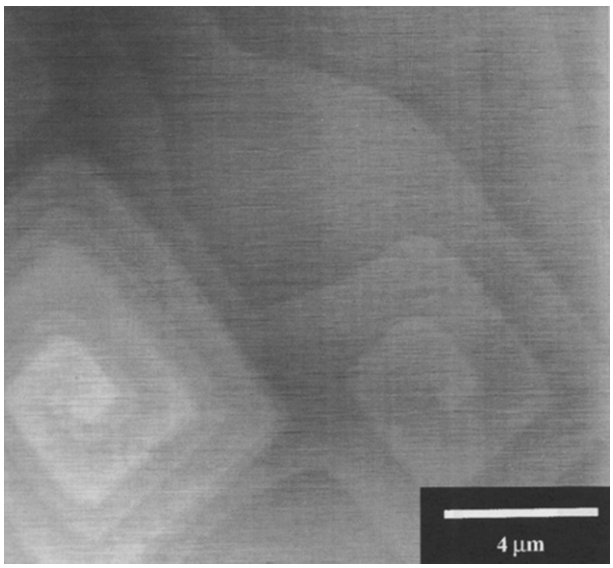

Fig. 17 Spiral growth observed in the AFM image of the natural zeolite heulandite.[27]

with a terrace height of 9 Å. This is a very curious phenomenon because the inevitable screw dislocation which runs through the crystal at the locus of the spiral must result in the structure twisting around the screw dislocation and translating 9 Å. This seems impossible to conceive that the crystal can displace over just one unit cell. Which means that either there is a mesoscopic void which must pass through the crystal along the line of the dislocation or otherwise the re-linking of the crystal occurs over several unit cells with a massive disruption of the structure along the dislocation. This is an unresolved problem. A variety of other structures have been studied by AFM and the heights of the terraces observed for a number of these porous structures are shown in Fig. 18 (Anderson[28]). In all cases the height of the terrace is in accordance with an obvious repeat in the structure suggesting that there are preferred surface terminations (lowest energy surfaces).

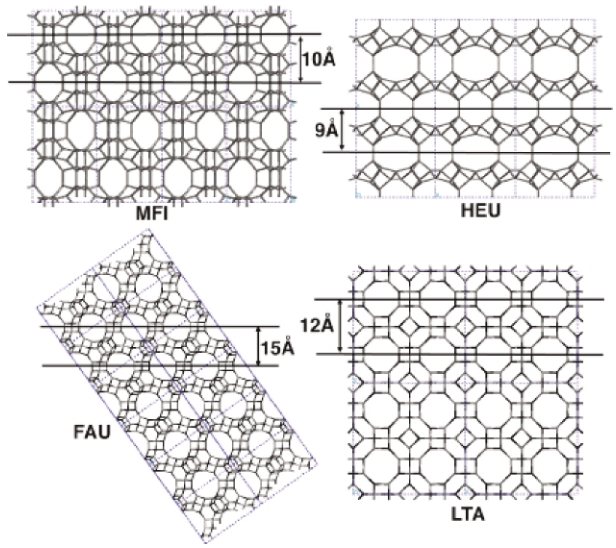

Fig. 18 Terrace heights observed by AFM for a variety of zeolite phases relate closely with natural cleavage planes.[28]

Zeolite A has been studied extensively by atomic force microscopy and reveals a layer type growth mechanism with terraces 12 Å in height, see Fig. 19 — Agger *et al.*[29] and Agger *et al.*[30] In zeolite A there is quite a high degree of surface nucleation. This results in many terraces with a square nature (the diamond shape is caused by tilt of the crystal in the microscope). The edges of the terraces run parallel to the edges of the crystals and when the terraces merge they create a curved growth front between these terraces. There is a lot of information in such a micrograph concerning the relative rates of growth processes in a zeolite and these can be determined by simulation of the AFM images using a particular growth model. Fig. 20 shows the definition of growth sites on the crystal surface in much the same vein as might be described for a dense phase crystal in terms of surface sites, edge sites and kink sites. However, the definition of sites takes on quite a different meaning for an open-framework porous material. The argument is based upon the criterion that the crystal has preferred terminations, both for the surface and for the edge of terraces. This is evidenced by the fact that many materials exhibit terraces with very well defined shapes. This is circumstantial evidence that the crystal grows in a step-wise manner — an example may be that a cage grows and then the structure is slightly more stable. The units of growth could be monomers, dimers or cages, the AFM gives no evidence on this issue, however, whatever the growth units the structure has stable surface structures. The surface, edge and kink site terminology therefore refers to the sites for complete addition of the smallest stable structure (not the actual growth unit). On this basis simulations of AFM images yield information about the relative stabilities of the different surface terminations – a surface site is more stable than an edge site is more stable than a kink site. On this basis Fig. 21 shows a montage of images from a simulation where the surface site is 500 times less likely to grow than a kink site and the edge site 15 times less likely than the kink site. All the features of the AFM images are reproduced by this simulation. One other recent report of high-resolution SEM using Cr-sputtering of samples is interesting because it was possible to decorate the terrace edges in a manner that made the edges easily visible in the SEM (see Fig. 22) — Bazzana *et al.*[31] Although this technique is perhaps less desirable than the ultra-high resolution work described in the previous section which, requires no sputtering, it could prove a useful technique for rapid scanning of growth features in porous materials.

Zeolite Y, with the faujasite (FAU) structure has also been studied AFM, Anderson *et al.*[32] Typical crystals have octahedral habit and Fig. 23 shows AFM on the triangular (111) facet. The right figure shows a typical surface structure for a crystal of aluminosilicate zeolite Y prepared under basic hydrothermal conditions. Triangular facets are observed with a height of 15 Å corresponding to a faujasite layer. Interestingly the orientation of the layers is opposite to that of the edges of the crystal face. When the same structure is formed but as a zinco-phosphate using a reverse micelle preparation to control gel speciation the surface structure is as shown on the right of Fig. 23 — Singh *et al.*[33] Again triangular terraces are observed, 15 Å in height but they have orientation the same as the crystal edges. This gross difference in the orientation of the terraces must be the result of a different growth mechanism and the discussion of this phenomena will be the focus of a modelling study soon to be published — Agger *et al.*[34]

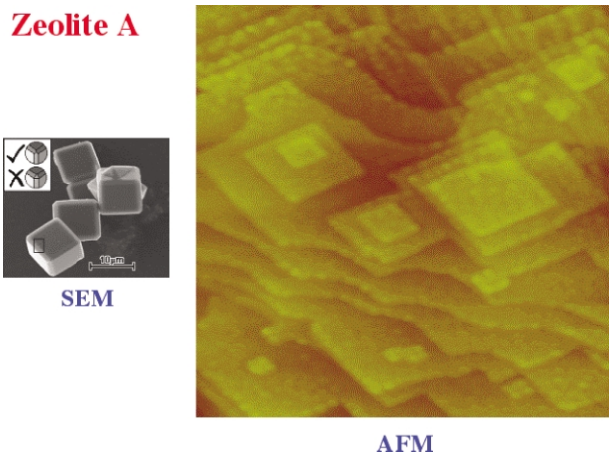

Fig. 19 12 Å high terraces observed on the [100] surface of zeolite A. Curved growth fronts relate to preferential growth at kink sites.[29,30]

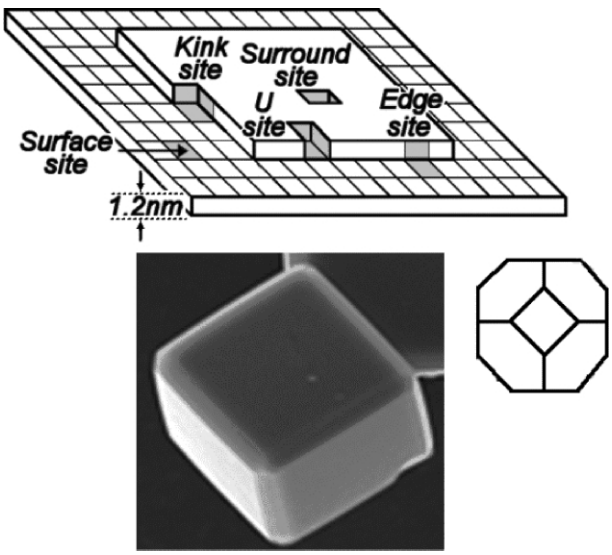

Fig. 20 Definition of growth sites on the surface [100] surface of zeolite A.[30]

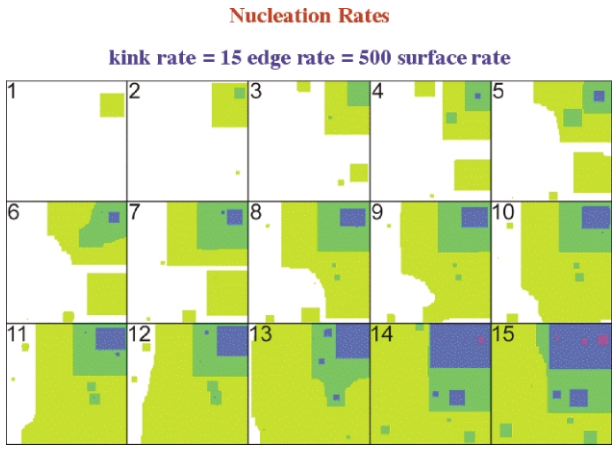

Fig. 21 Montage of calculated zeolite A surface structures based upon different probabilities of fundamental growth processes.[30]

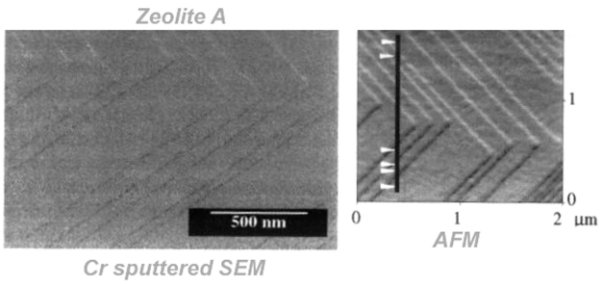

Fig. 22 SEM of Cr-sputtered zeolite A and corresponding AFM image both revealing 12 Å high surface terraces.[31]

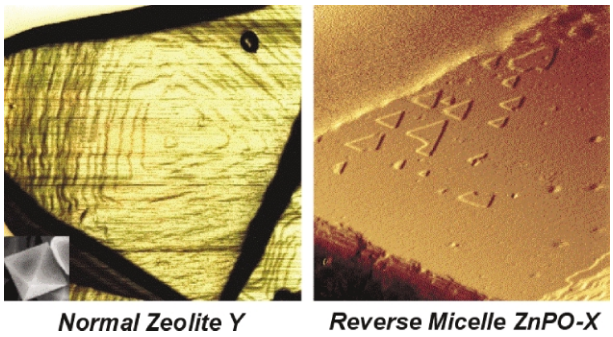

Fig. 23 Triangular terraces growing on the triangular (111) facet of faujasite type crystals. Depending on the synthesis conditions the triangles have opposite orientation indicating different growth mechanism.[32,33]

There is a keen desire always to perform characterisation experiments under in situ conditions and, as was mentioned previously, this should ultimately be possible in AFM studies of growth in porous materials. One reason is that the conditions when the crystals are removed from the growth nutrient will affect the final form of the crystal surface. At the end of a zeolite preparation, for instance, the supersaturation in the growth medium drops. This is likely to affect, in particular, surface nucleation which is the hardest process energetically and requires the highest level of supersaturation. This effect is demonstrated in Fig. 24 which shows

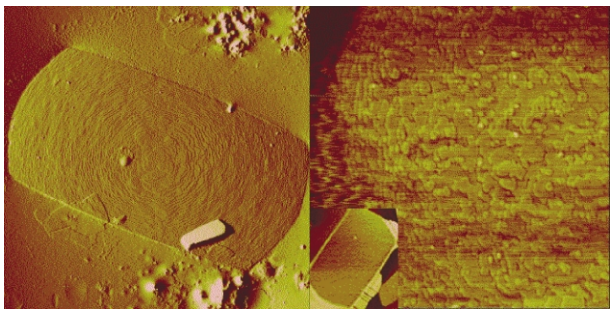

Fig. 24 Silicalite crystals, left at low supersaturation showing a low degree of surface nucleation and right at high supersaturation showing a high degree of surface nucleation.[35,36]

crystals of silicalite — Agger *et al.*[35,36] On the left the crystals have been removed from the synthesis when the supersaturation level had dropped and the crystals on the right are when the supersaturation is kept high by continual addition of nutrient during crystallisation. It is clear that when the supersaturation level is kept high there is a lot of surface nucleation and many small terraces whereas when the supersaturation level is low surface nucleation has almost stopped and the remaining terraces are growing out. This is very useful information because it gives a possibility to control surface nucleation *versus* spreading by controlling supersaturation levels.

Conclusion

In conclusion modern microscopy methods are now very powerful to address many problems in materials science and particularly to the study of nano-porous materials. Indeed they are a crucial tool in the arsenal of scientists wishing to understand structure and growth in such materials. Some of the techniques are more specialised, such as electron crystallography, but others such as high-resolution SEM and AFM should be available in most research laboratories in the near future. Consequently, we hope we have whetted the appetite to use microscopy methods more widely in the study of this exciting class of material.

Notes and references

1 J. M. Thomas, O. Terasaki, P. L. Gai, W. Zhou and J. Gonzalez-Calbet, *Acc. Chem. Res.*, 2001, **34**, 583.
2 A. Carlsson, T. Oka, J.-O. Bovin, G. Karlsson, Y. Okamoto, N. Ohnishi and O. Terasaki, *Chem. Eur. J.*, 1999, **5**, 244.
3 P. Wagner, O. Terasaki, S. Ritsch, J. G. Nery, S. I. Zones, M. E. Davis and K. Hiraga, *J. Phys. Chem. B*, 1999, **103**, 8245.
4 Z. Liu, T. Ohsuna, O. Terasaki, M. A. Camblor, M.-J. Diaz-Cabaòas and K. Hiraga, *J. Am. Chem. Soc.*, 2001, **123**, 5370.
5 T. Ohsuna, Z. Liu, O. Terasaki, K. Hiraga and M. A. Camblor, *J. Phys. Chem. B*, 2002, **106**, 5673.
6 Y. Sakamoto, M. Kaneda, O. Terasaki, D. Y. Zhao, J. M. Kim, G. D. Stucky, H. J. Shin and R. Ryoo, *Nature*, 2000, **408**, 449.
7 S. Che, Y. Sakamoto, O. Terasaki and T. Tatsumi, *Chem. Mater.*, 2001, **13**, 2237.
8 D. Weaire and R. Phelan, *Phil. Mag. Lett.*, 1994, **69**, 107.
9 M. W. Anderson, C. C. Egger, G. J. T. Tiddy and J. L. Casci, *Stud. Surf. Sci. Catal.*, 2002, **142**, 1149.
10 Y. Sakamoto, I. Diaz, O. Terasaki, D. Y. Zhao, J. Pèrez-Pariente, J. M. Kim and G. D. Stucky, *J. Phys. Chem. B*, 2002, **106**, 3118.
11 V. Alfreddson and M. W. Anderson, *Chem. Mater.*, 1996, **8**, 1141.
12 M. Kaneda, T. Tsubakiyama, A. Carlsson, Y. Sakamoto, T. Ohsuna and O. Terasaki, *J. Phys. Chem. B*, 2002, **106**, 1256.
13 R. Ryoo, S. Jun and J. M. Kim, *Chem. Commun.*, 1998, 2225.
14 O. Terasaki, Z. Liu, T. Ohsuna, H. J. Shin and R. Ryoo, *Microsc. Microanal.*, 2002, **8**, 35.
15 J. Miao, T. Ohsuna, O. Terasaki, K. O. Hodgson and M. W. O Keefe, *Phys. Rev. Lett.*, 2002, **89**, 155502.
16 A. J. Koster, U. Ziese, A. J. Verkleij, A. H. Janssen and K. P. de Jong, *J. Phys. Chem. B*, 2000, **104**, 9368.
17 A. H. Janssen, A. J. Koster and K. P. de Jong, *Angew. Chem., Int. Ed.*, 2001, **40**, 1102.
18 A. H. Janssen, A. J. Koster and K. P. de Jong, *J. Phys. Chem. B*, 2002, **106**, 11905.
19 P. A. Midgley, M. Weyland, J. M. Thomas and B. F. G. Johnson, *Chem. Commun.*, 2001, 907.
20 M. Weyland, P. A. Midgley and J. M. Thomas, *J. Phys. Chem. B*, 2001, **105**, 7882.
21 P. A. Midgley, M. Weyland, J. M. Thomas, P. L. Gai and E. D. Boyes, *Angew. Chem., Int. Ed.*, 2002, **41**, 3804.
22 A. H. Janssen, P. Van Der Voort, A. J. Koster and K. P. de Jong, *Chem. Commun.*, 2002, 1632.
23 S. N. Che, K. Lund, T. Tatsumi, S. Iijima, S. H. Joo, R. Ryoo and O. Terasaki, *Angew. Chem., Int. Ed.*, 2003, **42**, 2182.
24 V. Alfredsson, T. Ohsuna, O. Terasaki and J.-O. Bovin, *Angew. Chem., Int. Ed. Engl.*, 1993, **32**, 1210.
25 T. Ohsuna, Y. Horigawa, K. Hiraga and O. Terasaki, *Chem Mater.*, 1998, **10**, 688.
26 B. Slater, C. R. A. Catlow, Z. Liu, T. Ohsuna, O. Terasaki and M. Camblor, *Angew. Chem., Int. Ed.*, 2002, **41**, 1235.
27 S. Yamamoto, S. Sugiyama, O. Matsuoka, T. Honda, Y. Banno and H. Nozoye, *Microporous Mesoporous Mater.*, 1998, **21**, 1.
28 M. W. Anderson, *Current Opinion in Solid State and Materials Science*, 2001, **5**, 407.
29 J. R. Agger, N. Pervaiz, A. K. Cheetham and M. W. Anderson, *J. Am. Chem. Soc.*, 1998, **120**, 10754.
30 J. R. Agger, N. Hanif and M. W. Anderson, *Angew. Chem., Int. Ed. Engl.*, 2001, **40**, 4065.
31 S. Bazzana, S. Dumrul, L. Hsiao, L. Klass, M. Knapp, J. A. Rains, E. M. Stein, M. J. Sullivan, C. M. West, J. Y. Yoo and A. Sacco Jr., *Stud. Surf. Sci. Catal.*, 2002, **142**, 117.
32 M. W. Anderson, J. R. Agger, J. T. Thornton and N. Forsyth, *Angew. Chem., Int. Ed. Engl.*, 1996, **35**, 1210.
33 R. Singh, J. Doolittle, M. A. George and P. K. Dutta, *Langmuir*, 2002, **18**, 8193.
34 J. R. Agger, M. W. Anderson, N. Hanif and P. K. Dutta, in preparation.
35 J. R. Agger, N. Hanif, C. S. Cundy, A. Wade and M. W. Anderson, *J. Am. Chem. Soc.*, 2003, **125**, 830.
36 M. W. Anderson, C. S. Cundy, S. Dennison, P. A. Rawlinson and J. R. Agger, in preparation.